24th ABCM International Congress of Mechanical Engineering
December 3-8, 2017, Curitiba, PR, Brazil

# COBEM-2017-1917
# FINITE ELEMENT ANALYSIS OF A SHAPE MEMORY ALLOY HONEYCOMB VIBRATION ABSORBER

**Gabriel Guimarães Averbug**
**Antonio Candido Rapozo**
CEFET/RJ – Centro Federal de Educação Tecnológica Celso Suckow da Fonseca - Department of Mechanical Engineering,
Av. Maracanã, 229 – Maracanã, Rio de Janeiro – RJ, 20271-110
averbugg@gmail.com, rapozoantonio@gmail.com

**Pedro Manuel Calas Lopes Pacheco**
CEFET/RJ – Centro Federal de Educação Tecnológica Celso Suckow da Fonseca - Department of Mechanical Engineering,
Av. Maracanã, 229 – Maracanã, Rio de Janeiro – RJ, 20271-110
pedro.pacheco@cefet-rj.br

**Ricardo Alexandre Amar de Aguiar**
CEFET/RJ – Centro Federal de Educação Tecnológica Celso Suckow da Fonseca - Department of Mechanical Engineering,
Av. Maracanã, 229 – Maracanã, Rio de Janeiro – RJ, 20271-110
ricardoaamar@yahoo.com.br

**Marcelo Amorim Savi**
Universidade Federal do Rio de Janeiro
COPPE – Department of Mechanical Engineering
Center for Nonlinear Mechanics
P.O. Box 68.503 – 21.941.972 – Rio de Janeiro – RJ – Brazil
savi@mecanica.coppe.ufrj.br

***Abstract.*** *Shape memory alloys (SMAs) are smart materials with the ability of modifying their initial shape as a response to mechanical or thermal loads. As a consequence of their complex thermomechanical behavior associated with phase transformation, SMAs are able to generate significant forces and displacements. Pseudoelastic effect occurs in austenitic SMAs, which present hysteretic behavior associated with energy dissipation developed during a loading-unloading cycle. Therefore, SMA elements can be used as vibration absorbers. Since both geometric and constitutive nonlinearities take place, the design of shape memory alloys vibration absorbers presents several challenges. This work presents a numerical model based on the finite element method developed to study the energy dissipation capability of an SMA absorber connected to plates to form a honeycomb structure. The proposed methodology aims the investigation of S-shaped modular geometries with pseudoelastic elements, which can be used as efficient absorbers for vibration reduction. A constitutive model with internal variables describes the pseudoelastic behavior of SMAs.*

*Keywords: shape memory alloys, pseudoelasticity, vibration absorbers, honeycomb structures, finite element method.*

## 1. INTRODUCTION

Shape memory alloys (SMAs) are smart materials, which are able to perform large forces and displacements under thermomechanical loads due to their complex behavior associated with phase transformation (Lagoudas, 2008). Two main phases are presented on SMAs: austenite and martensite. The thermomechanical properties of SMAs make them appropriate for several applications, such as in aerospace, automotive industry, biomedicine and robotics (Lagoudas, 2008; Nava et al, 2014; Jani et al, 2013). Shape memory effect and pseudoelasticity are the two main phenomena present in these materials, both associated to phase transformation promoted either by mechanical or thermal loads. Pseudoelasticity takes place in SMAs at high temperatures, above a critical temperature ($A_F$), where austenite is the stable phase in a stress-free state. Figure 1 shows a stress-strain curve for the pseudoelastic response of an SMA specimen. As a result of the hysteretic behavior, SMAs are able to dissipate mechanical energy in each loading-unloading cycle, making them appropriate to be used for vibration attenuation purposes (Lagoudas, 2008; Nava *et al.*, 2014; Jani *et al.*, 2013; Johnson *et al.*, 2008).

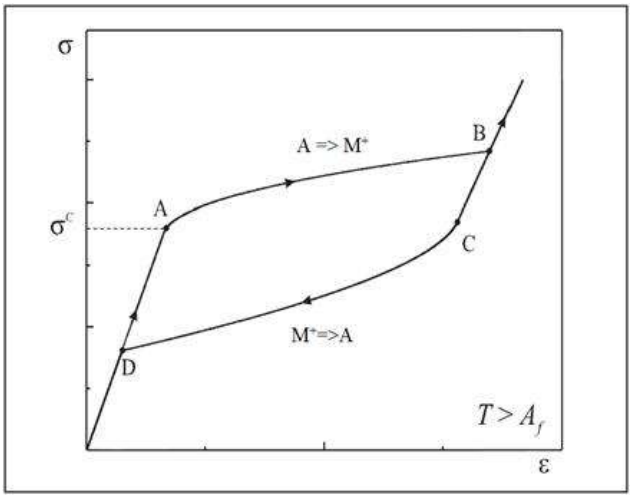


Figure 1 – Stress-strain curve for pseudoelastic behavior of SMAs

## 2. COMPUTATIONAL PROCEDURE

The proposed work presents a numerical investigation of SMA absorbers based on the finite element method. The idea is to analyze the energy dissipation capability behavior of a SMA vibration absorber connected to plates to form a honeycomb structure.

Figure 2 shows S-shaped SMA elements, displayed by the dark blue color, and the plates, displayed by the purple color. The plates represent a structure connected to several repeated regular SMA absorbers, producing a low-density periodic structure, such as a honeycomb. ANSYS software (ANSYS, 2018) is used for finite element simulations. A quasi-static analysis is performed by applying a prescribed loading-unloading vertical displacement to the structure and results are evaluated considering hysteresis loop and energy dissipation associated with each cycle.

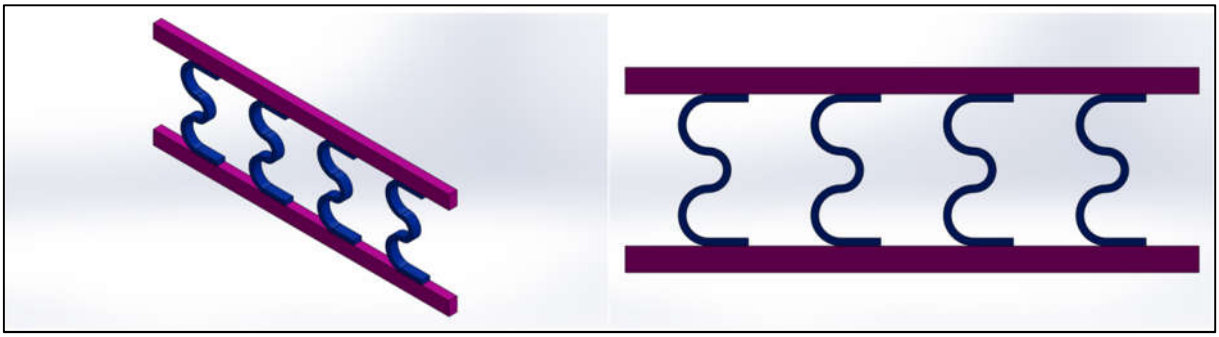

Figure 2 – SMA vibration absorber in a honeycomb structure.

A study using S-shaped modular geometries with pseudoelastic plane elements is performed to evaluate the influence of geometric parameters on the system response. Figure 3 shows the simplest geometry used, which corresponds to a one fold SMA element with parameterized dimensions. This geometry is called module and is used to compose more complex geometries by increasing the number of folds.

Figure 4 presents some examples of other geometries analyzed in the study. In order to evaluate the influence of loading direction on the dynamic response of the system, different geometries under compressive and tensile loads were analyzed. The geometric parameters employed are: the number of folds ($n$) and the index ($i$), defined by the ratio between the SMA element arc radius $R$ and the thickness $t$. Table 1 and Tab. 2 present all the numerical cases performed in present work.

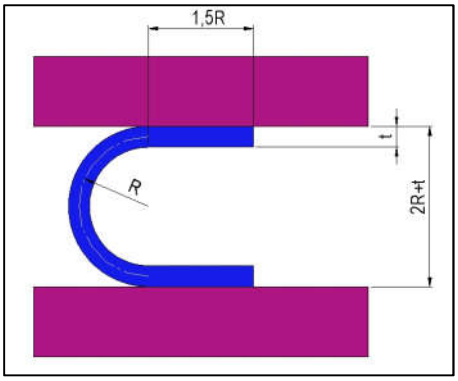


Figure 3 – Geometry with one fold containing the parameterized dimensions (module).

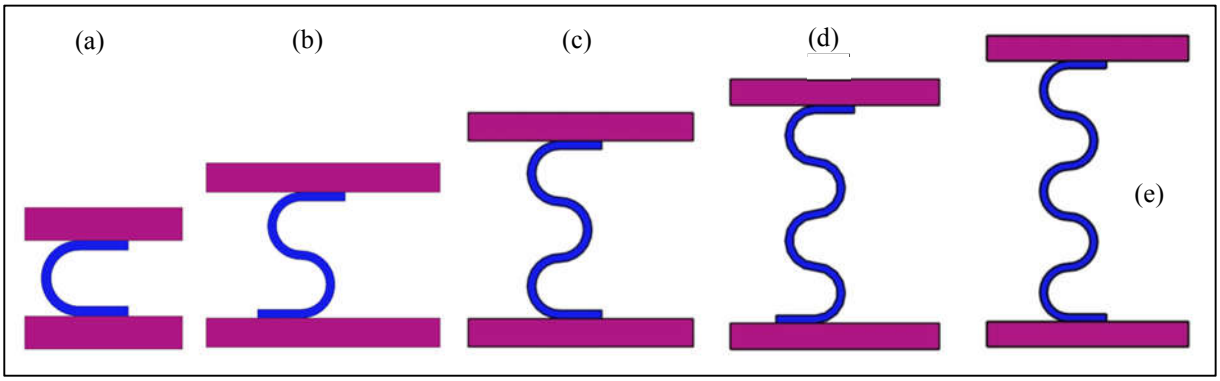


Figure 4 – S-shaped geometries with one (a), two (b), three (c), four (d) and five (e) folds.

Table 1 – Numerical cases under compression

| COMPRESSION | |
|---|---|
| **Number of folds (*n*)** | **index (*i*)** |
| 1 | 4 |
| | 3 |
| | 2 |
| 2 | 4 |
| | 3 |
| | 2 |
| 3 | 4 |
| | 3 |
| | 2 |
| 4 | 4 |
| | 3 |
| | 2 |
| 5 | 4 |
| | 3 |
| | 2 |
| 6 | 4 |
| | 3 |
| | 2 |
| **Total number of cases** | 18 |

Table 2 – Numerical cases under tension

| TENSION | |
|---|---|
| **Number of folds (*n*)** | **index (*i*)** |
| 1 | 4 |
| | 3 |
| | 2 |
| | 1,5 |
| | 1,0 |
| | 0,75 |
| 2 | 4 |
| | 3 |
| | 2 |
| | 1,5 |
| | 1,0 |
| | 0,75 |
| 3 | 4 |
| | 3 |
| | 2 |
| | 1,5 |
| | 1,0 |
| | 0,75 |
| 4 | 4 |
| | 3 |

| TENSION | |
|---|---|
| Number of folds (*n*) | index (*i*) |
| | 2 |
| | 1,5 |
| | 1,0 |
| | 0,75 |
| 5 | 4 |
| | 3 |
| | 2 |
| | 1,5 |
| | 1,0 |
| | 0,75 |
| 6 | 4 |
| | 3 |
| | 2 |
| | 1,5 |
| | 1,0 |

| TENSION | |
|---|---|
| Number of folds (*n*) | index (*i*) |
| | 0,75 |
| 7 | 4 |
| | 2 |
| | 0,75 |
| 8 | 4 |
| | 2 |
| | 0,75 |
| 9 | 4 |
| | 2 |
| | 0,75 |
| 10 | 4 |
| | 2 |
| | 0,75 |
| **Total number of cases** | 48 |

Several constitutive models that represent the thermomechanical behavior of SMAs are available in the current literature (Lagoudas, 2008; Nava *et al.*, 2014; Jani *et al*., 2013; Johnson *et al.*, 2008; Auricchio *et al*., 2004; Paiva *et al*., 2006). In order to describe SMA thermomechanical behavior, the constitutive model proposed by Auricchio and Petrini (2004) is employed. This phenomenological model with internal variables is able to reproduce both pseudoelastic and shape memory alloy effects.

Figure 5 presents a schematic representation of the parameters of Auricchio and Petrini (2004) constitutive model. $E_A$ and $E_M$ represent the elasticity modulus of austenite and martensite, respectively, and satisfy the following relation $E_A + \xi_M(E_M - E_A)$, where $\xi_M$ is the volume fraction of martensite. $\varepsilon_L$ represents the maximum transformation strain and $R$ is the radius of the elastic domain, which graphically represents the width and the half height of the hysteresis loop, respectively. $h$ is the material parameter defining the slope of the linear stress-transformation strain relation, $\beta$ corresponds to a parameter related to the dependency of the critical stress on temperature and $T_0$ is the reference temperature. Finally, $m$ represents the Lode dependency factor and is defined by Eq. (1):

$$m = \sqrt{\frac{27}{2}}\frac{\sigma_c - \sigma_t}{\sigma_c + \sigma_t} \tag{1}$$

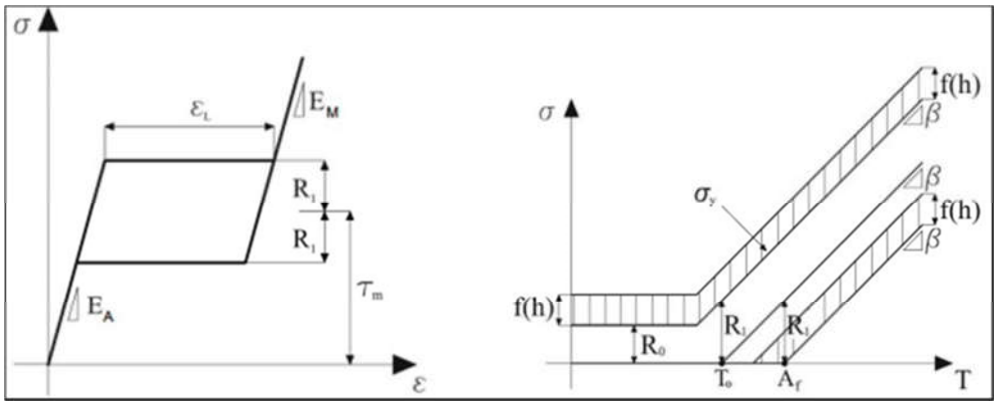


Figure 5 – Graphical representation of the constitutive parameters of Auricchio and Petrini (2004) model

The numerical model was calibrated using the experimental data from Xie (2016), which performed tensile tests in rectangular cross section pseudoelastic SMA samples to analyze the influence of loading rate on the material behavior. Calibration process consists of comparing the results of a numerical model of a tensile test with the same conditions as in the experiment performed by Xie (2016). The constitutive parameters obtained after a calibration process can be seen in Tab. 3.

Table 3 – Constitutive parameters obtained from Xie (2016) after a calibration process.

| Parameter | Value |
|---|---|
| $h$ (GPa) | 11,50 |
| $T0$ (K) | 273,95 |
| $R$ (MPa) | 60,50 |
| $\beta$ (MPa/K) | 4,20 |
| $\varepsilon L$ (-) | 0,046 |
| $EM$ (GPa) | 21,61 |
| $m$ (-) | 0 |

## 3. RESULTS AND DISCUSSION

Results generated by the numerical simulations are assessed according to two different analysis parameters: the first concerning the energy dissipation capability of the system, the dissipated energy per volume unit ($\gamma$), and the second regarding the system dynamic behavior, the average stiffness ($\overline{K}$). The dissipated energy per unit volume $\gamma$ is defined by the ratio between the dissipated energy of each cycle, calculated by the area inside the hysteresis loop, and the volume of the geometry analyzed. The average stiffness $\overline{K}$ is analyzed qualitatively by the slopes of the linear regions in the stress-strain curves, which represent the stiffness of both austenitic and martensitic phases.

The first study evaluates the influence of the parameter index $i$ on $\gamma$ and $\overline{K}$. Figure 6 and Fig. 7 present $F \times u$ and $\gamma \times i$ curves for the geometries with 1 fold ($n$ = 1) and 6 folds ($n$ = 6) under tensile loading, respectively. In both cases one can see that the average stiffness $\overline{K}$ tends to decrease as the index $i$ increases due to the thickness reduction of the SMA element. Furthermore, there is a clear growth tendency of $\gamma$ as $i$ increases for the geometries with $n$ = 6, which is roughly linear, as can be observed in Fig. 7 (b). However, the geometries with $n$ = 1 present a non-monotonic behavior at $i$=0.75, as showed by Fig. 6 (b).

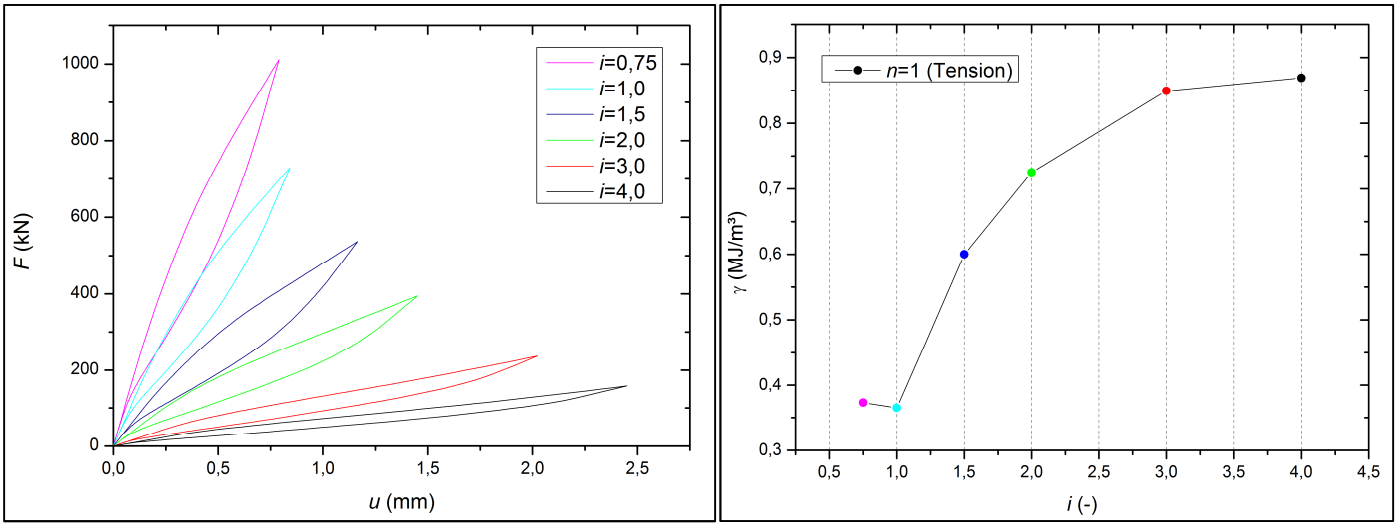


(a) (b)

Figure 6 – Force-displacement (a) and $\gamma$ versus $i$ (b) curves for the geometries with 1 fold under tensile loading

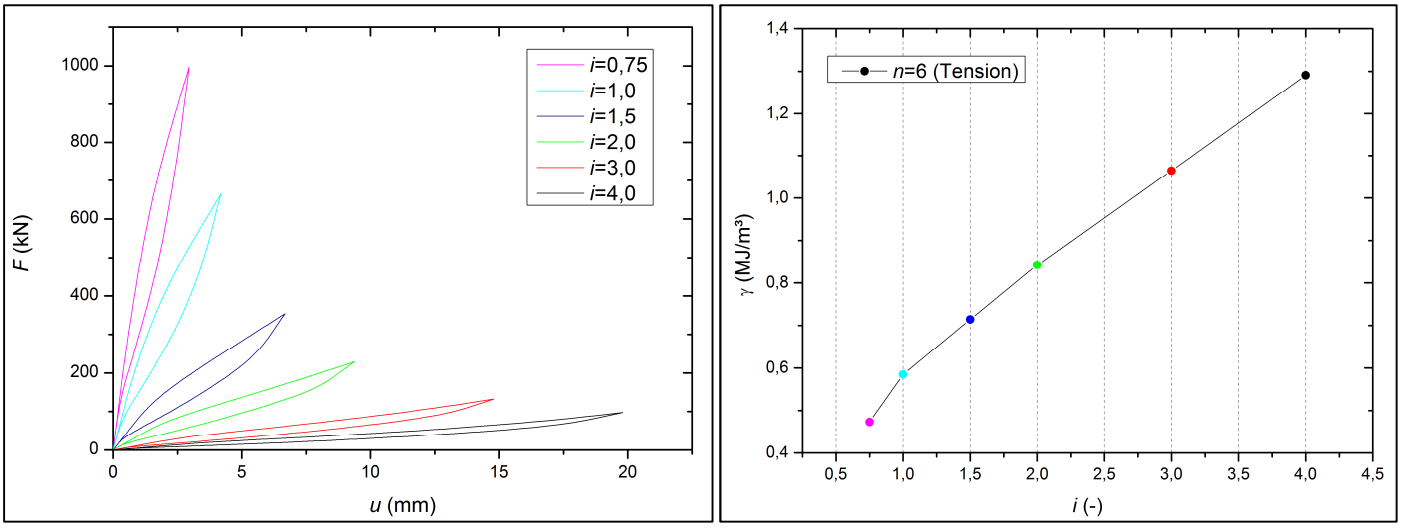


(a) (b)

Figure 7 – Force-displacement (a) and $\gamma$ versus $i$ (b) curves for the geometries with 6 folds under tensile loading

The second study intends to access the influence of the number of folds $n$ on $\gamma$ and $\overline{K}$. Figure 8 presents $F \times u$ and $\gamma \times i$ curves for all geometries with $i = 2$ under tensile loading. The analysis of Fig. 8 (a) reveals that the average stiffness $\overline{K}$ is reduced with the increasing number of folds, since the structure tends to be more flexible. Figure 8 (b) exhibits a monotonic growth of $\gamma$ from $n = 3$ to $n = 10$, which gradually stabilizes as the number of folds becomes bigger. However, the results at $n = 1$ and $n = 2$ present a different behavior in comparison with the other geometries.

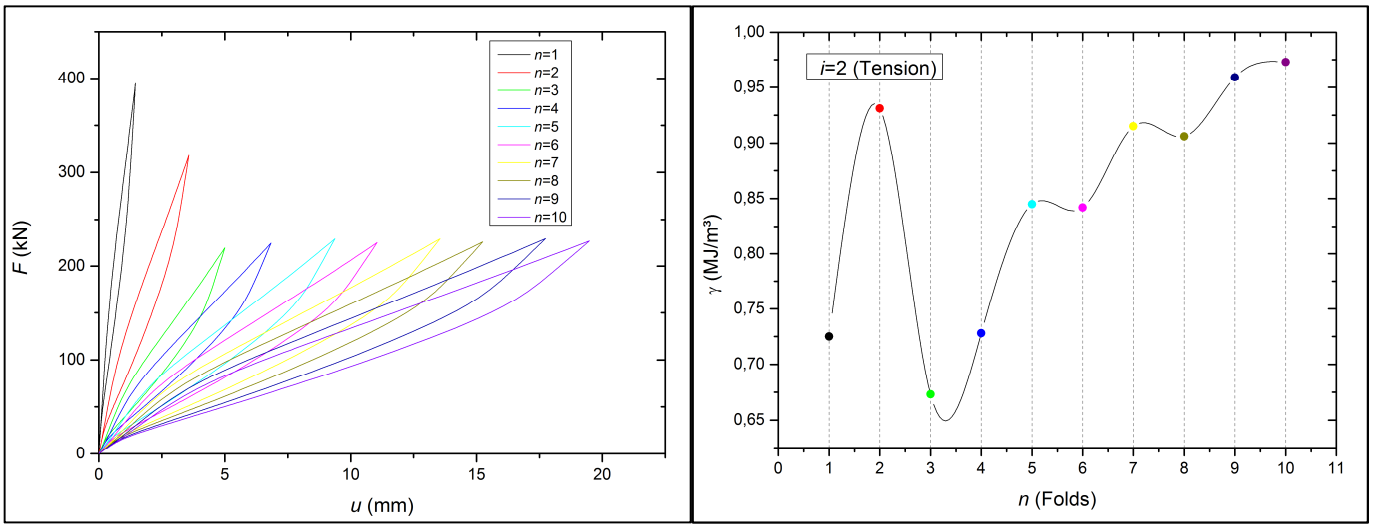


(a) (b)

Figure 8 – Force-displacement (a) and $\gamma$ versus $n$ (b) curves for the geometries with $i$=2 under tensile loading

Figure 9 presents a curve, which relates normalized dissipated energy and volume to the number of folds $n$. The normalized dissipated energy is defined by $\frac{E_n}{E_{n_1}}$, where $E_n$ represents the dissipated energy of a geometry with a given number of folds $n$ and $E_{n_1}$corresponds to the dissipated energy of the geometry with 1 fold. The same concept is used for the normalized volume. As it can be seen in Fig. 9, there is an initial leap of the dissipated energy in comparison to the volume at $n = 2$, which emphasizes the unusual behavior of this particular geometry. At $n = 2$ the absolute value of dissipated energy represents the only condition where it is larger than the following value as $n$ increases, in other words, larger than the one at $n = 3$. However, as $n$ grows from $n = 3$, the dissipated energy tends to increase proportionally more than the volume, which can be concluded by the gradual deviation of both black and red curves.

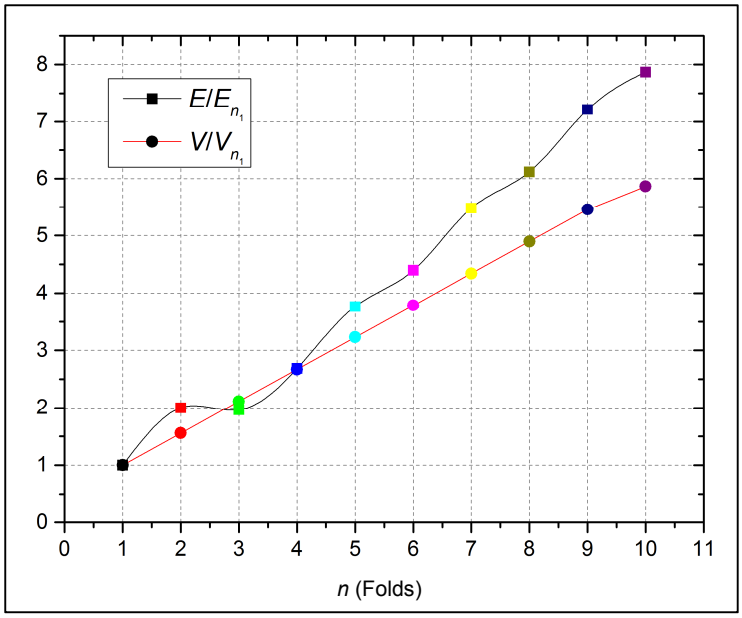


Figure 9 – Normalized dissipated energy and volume versus number of folds curves for the geometries with *i*=2 under tensile loading

Figure 10 and Fig. 11 present the plots illustrating, respectively, the *von Mises* stress and volume fraction of martensite distributions for 1 fold and 10 folds geometries with *i*=2 under tensile loading. The analyses of the plots reveal that, as expected, the regions with higher values of stress concentration correspond to the ones with higher values of volume fraction of martensite. It can be also observed that the 1 fold geometry presents significant values of volume fraction of martensite in the region of interface between the plate and the SMA element, which tends to disappear as the structure becomes less rigid, as it can be seen in the example of the 10 folds geometry. Since the absolute value and concentration of volume fraction of martensite in the 1 fold geometry are larger than the ones of the other geometries, $\gamma$ becomes also larger, what could explain the non-monotonic behavior showed by Fig. 8 (b) and Fig. 9.

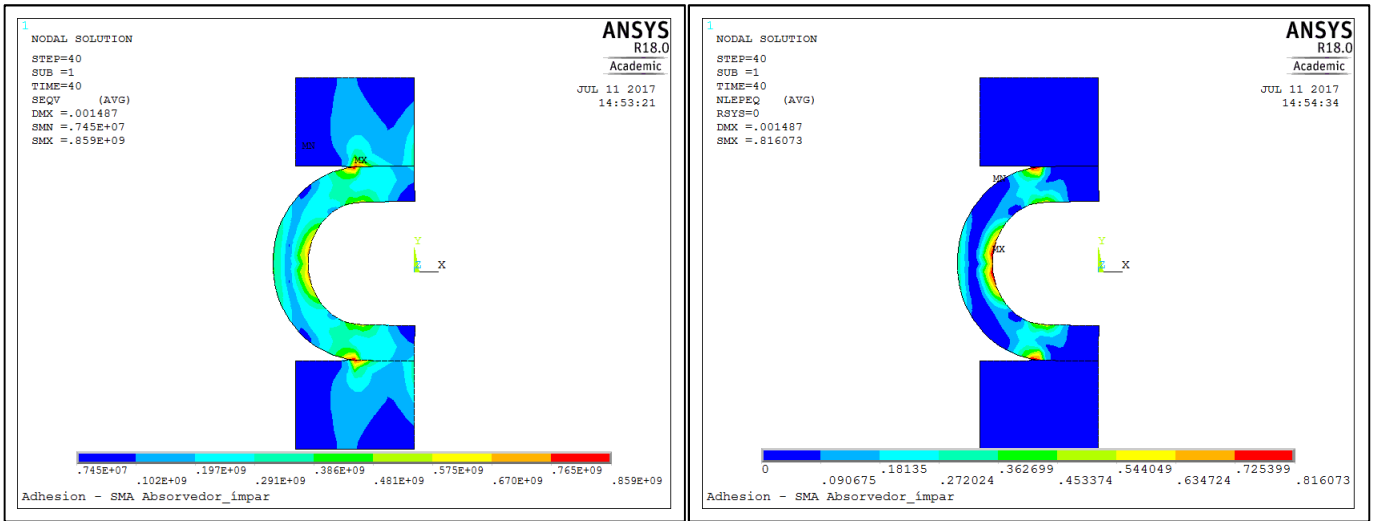


(a) (b)

Figure 10 – Von Mises stress (a) and volume fraction of martensite (b) plots for a 1 fold geometry with *i*=2 under tensile loading

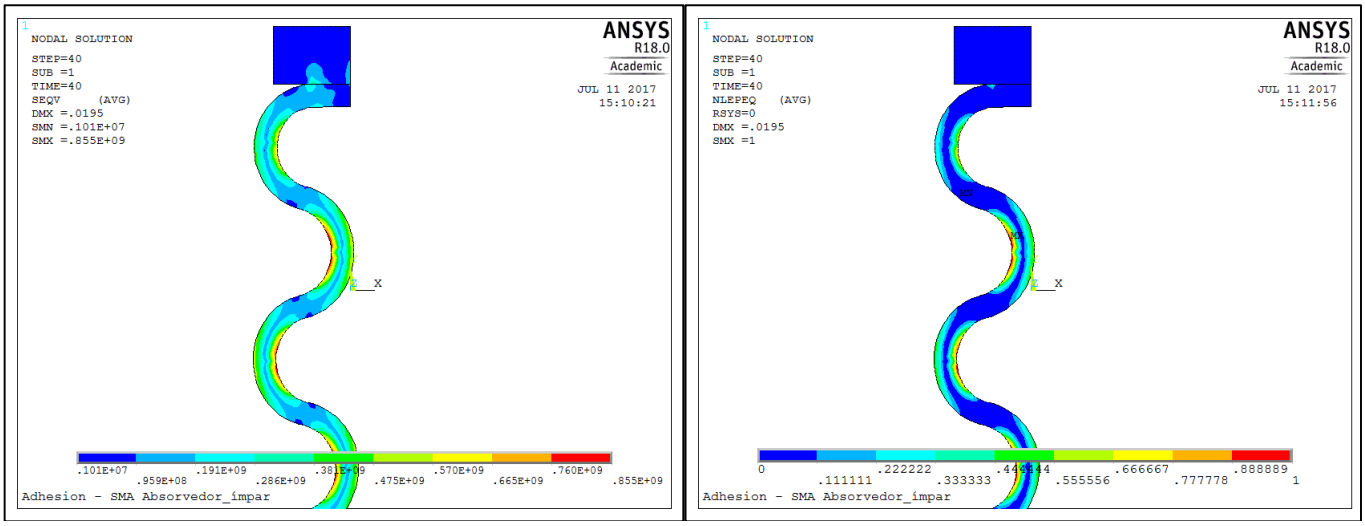


(a) (b)

Figure 11 – *von Mises* stress (a) and volume fraction of martensite (b) distribution for a 10 folds geometry with $i$=2 under tensile loading

The third and last study evaluates the loading direction (tension and compression) influence on $\overline{K}$. Figure 12 presents the force-displacement curves for the geometries with 1 fold and 5 folds, where the solid line represents the tensile loading and the dotted line represents the compressive loading. One can see that, as the structure stiffness becomes smaller and the applied displacements increase, whether by increasing the number of folds $n$ or the index $i$, the difference between the hysteresis loops under tension and compression stands out due to the geometric non-linearities.

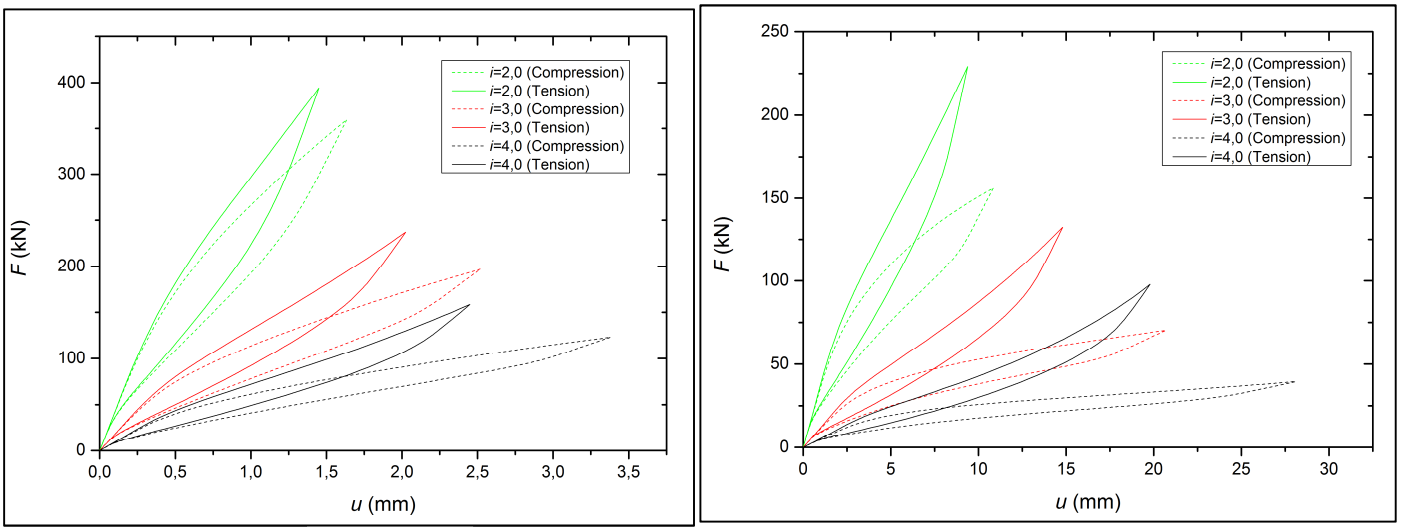


(a) (b)

Figure 12 – Force-displacement curves for the geometries with 1 fold (a) and 5 folds (b)

The influence of the geometric non-linearities in the loading direction can be better understood by the analysis of the final strained configurations, as it can be seen in Fig. 13. One can see that the final strained configuration under tension tends to reproduce the behavior of a beam, which is much more rigid than the final strained configuration under compression, which tends to reproduce the behavior of a spring. This is the reason for the hysteresis loop translation under different loading directions observed in Fig. 12.

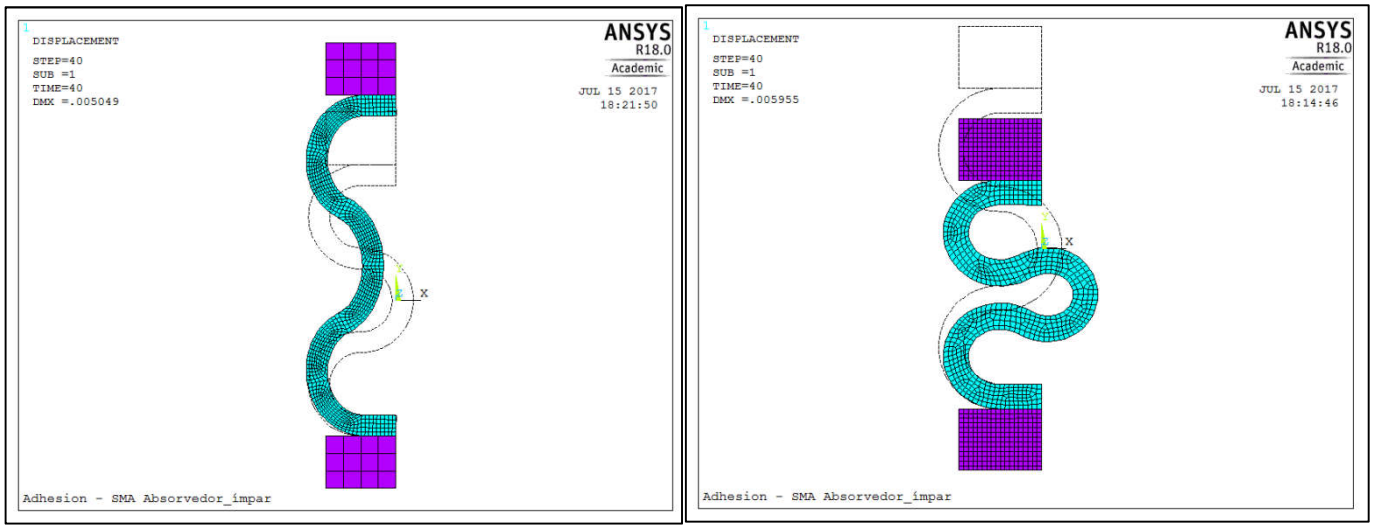


(a) (b)

Figure 13 – Final strained configuration under tensile (a) and compressive (b) loading

## 4. CONCLUSIONS

Hysteretic behavior is related to energy dissipation, making the use of pseudoelastic SMAs elements interesting for vibration attenuation purposes. A finite element model is developed to study the energy dissipation capability of different SMA honeycomb vibration absorbers geometries. The proposed model can be used as a tool for analyzing phase transformation distribution and to select geometries of SMA vibration absorbers in order to maximize the energy dissipation capability. The obtained results show that the proposed geometries offer an alternative to the construction of vibration absorbers with low-weighted SMA pseudoelastic elements with a wide range of dissipated energy and stiffness values. Furthermore, geometries with a larger number of folds and index tend to be more influenced by the geometric non-linearities, since they are subjected to larger displacements. Geometric non-linearities are also responsible for the remarkable behavior difference of the structure under tension and compression, which can be seen by the deviation of the hysteretic curves.

## 5. ACKNOWLEDGEMENTS

The authors would like to acknowledge the support of the Brazilian Research Agencies CNPq, CAPES and FAPERJ. The Air Force Office of Scientific Research (AFOSR) is also acknowledged.

## 6. REFERENCES

Auricchio, F., Petrini, L., 2004, *A three-dimensional model describing stress temperature induced solid phase transformations. Part I: solution algorithm and boundary value problem*, International Journal for Numerical Methods in Engineering, Vol.61, pp. 807-836.

Jani, J. M., Leary, M., Subic, A., Gibson, M. A., 2013, *A review of shape memory alloy research, applications and opportunities, Materials and Design*, Vol. 56, pp. 1078–1113

Johnson, R., Padgett, J. E., Maragakis, M. E., Desroches, R., Saiidi, M. S, 2008, *Large scale testing of Nitinol shape-memory alloy devices for retrofitting of bridges*, Smart Materials and Structures, Vol. 17, pp. 1-10.

Lagoudas, D. C, 2008, *Shape Memory Alloys – Modeling and Engineering Applications*, Springer, Texas.

Nava, N., Collado, M., Cabás, R., 2014, *New Pin Puller Based on SMA Technology for Space Applications*, Journal of Materials Engineering and Performance, Vol. 23(7), pp. 2712–2718.

Paiva, A., and Savi, M. A., 2006, *An Overview of Constitutive Models for Shape Memory Alloys. Mathematical Problems in Engineering*, Vol.2006, pp. 1-30.

Xie, X., Kan, Q., Kang, G., Lu, F., & Chen, K., 2016, *Observation on rate-dependent cyclic transformation domain of super-elastic NiTi shape memory alloy*,. Materials Science and Engineering, Vol.671, pp. 32-47.

## 7. RESPONSIBILITY NOTICE

The authors are the only responsible for the printed material included in this paper.